

UNCERTAINTIES IN MODELING HELICOPTER DYNAMICS: A FRAMEWORK APPLIED TO SYSTEM IDENTIFICATION RESULTS

Steffen Greiser
Steffen.Greiser@dlr.de
German Aerospace Center (DLR), Institute of Flight Systems
Lilienthalplatz 7, 38108 Braunschweig, Germany

ABSTRACT

Helicopters are heavily coupled, unstable and their modeling is often a difficult nut to crack. This often makes control design for the helicopter difficult. However, a goal for the near future for the EC135 Active Control Technology / Flying Helicopter Simulator (ACT/FHS) is high-performance control to assess the in-flight simulation capability. This stimulates the requirements for the feedback control design which is based on linear models derived by system identification. The core problem for this type of design is often a mismatch of the closed-loop behavior to measured flight test data. This paper focuses on the question how the design can be assisted to improve the plant's model, so that the gap between design and flight can be reduced. The framework relies on linear models derived by system identification. These linear models are stitched together to describe not only the operating point but also the flight envelope of interest. The linear models are also extended by non-physical models that describe the uncertainties. The model of the plant finally consists of two parts: the physics-based, stitched model and the non-physical uncertainties. Compared to the classical techniques system identification and nonlinear modeling, the framework proposed in this paper can be applied quickly and indicates possible model improvements. The paper shows the application of the whole framework to ACT/FHS flight test results.

NOTATION

<hr/> <p>ACT/FHS</p> <p>ATTheS</p> <p>a_x, a_y, a_z</p> <p>$\mathbf{A}_{11}, \mathbf{A}_{12},$ $\mathbf{A}_{21}, \mathbf{A}_{22}$</p> <p>$\mathbf{A}, \mathbf{B}, \mathbf{C}, \mathbf{D}$</p> <p>$\mathbf{B}_1, \mathbf{B}_2$</p> <p>$\mathbf{f}$</p> <p>$g$</p> <p>$G_{is,m}$</p> <p>$J_{RMS}$</p> <p>$K_d$</p> <p>$K_{dd}$</p> <p>$K_i$</p> <p>$K_p$</p> <p>$L, M, N$</p> <p>$p, q, r$</p> <p>RMS</p> <p>$s$</p> <p>$u, v, w$</p> <p>$u_b, v_b, w_b$</p>	<p>Active Control Technology / Flying Helicopter Simulator</p> <p>Advanced Technology Testing Helicopter System</p> <p>linear accelerations</p> <p>partitions of the system matrix \mathbf{A}</p> <p>linear state-space matrices</p> <p>partitions of the system matrix \mathbf{B}</p> <p>nonlinear system vector</p> <p>gravitation constant</p> <p>frequency response of the residual controls due to measured controls</p> <p>cost function, root mean square error</p> <p>differential gain</p> <p>gain for the 2^{nd} derivative</p> <p>integral gain</p> <p>proportional gain</p> <p>external moments</p> <p>angular velocities</p> <p>root mean square error</p> <p>Laplace variable</p> <p>body-axis velocities</p> <p>bounded body-axis velocities</p>	<p>\mathbf{u}, \mathbf{U}</p> <p>\mathbf{u}_c</p> <p>\mathbf{u}_f</p> <p>\mathbf{u}_{is}</p> <p>\mathbf{u}_m</p> <p>\mathbf{u}_t</p> <p>w_h</p> <p>\mathbf{x}</p> <p>\mathbf{x}_t</p> <p>$x_{ll} \ y_{ll}$</p> <p>X, Y, Z</p> <p>\mathbf{y}_r</p> <p>\mathbf{y}</p> <p>α, β</p> <p>Δ</p> <p>Δ_a</p> <p>Δ_m</p> <p>ξ</p> <p>ξ_f</p> <p>ξ_{PID}</p> <p>$\delta_x, \delta_y, \delta_p, \delta_0$</p> <p>$\phi, \theta$</p> <p>$\theta_c$</p> <p>$\omega$</p>	<p>control vector: time & frequency domain</p> <p>commanded controls by the feedback</p> <p>filtered controls \mathbf{u}_c</p> <p>inverse simulated controls</p> <p>measured controls</p> <p>vector of the trim controls</p> <p>non-physical state due to inflow</p> <p>state vector</p> <p>vector of the trim states</p> <p>lead-lag states</p> <p>external forces about the rotorcraft's center of gravity</p> <p>reference value</p> <p>outputs</p> <p>angle of attack and sideslip</p> <p>perturbation</p> <p>additive uncertainty</p> <p>input uncertainty</p> <p>interpolation variable, airspeed</p> <p>filtered interpolation variable ξ</p> <p>operating point $\xi = const.$</p> <p>longitudinal, lateral, pedal, collective control inputs</p> <p>roll and pitch angles</p> <p>commanded pitch angle</p> <p>frequency</p> <hr/>
--	--	---	---

1. INTRODUCTION

DLR (The German Aerospace Center) performs research on helicopter assistance and demonstrates the function with the research helicopter ACT/FHS (Active Control Technology / Flying Helicopter Simulator). One important aspect of the assistance system is feedback control which can be tested easily on the ACT/FHS. The EC135 ACT/FHS is a light, twin-engine helicopter with bearingless main rotor and Fenestron (see figure 1). Its mechanical controls are replaced by a full-authority fly-by-wire/fly-by-light primary control system, which allows changes of the control inputs applied to the actuators by an experimental system [1]. Because of these changes, the dynamic data shown in this paper are not comparable to data from series-production rotorcraft. The aircraft was developed jointly by Airbus Helicopters Germany, Liebherr Aerospace Lindenberg, the German Federal Office of Bundeswehr Equipment, Information Technology and In-Service Support, and DLR. It is owned and operated by DLR. The ACT/FHS permits operations with the core system (controlled by the safety pilot) and with the experimental system (controlled by the evaluation pilot). The core system meets the high civil aviation safety requirements with a catastrophic failure probability of 10^{-9} per flight hour. It features the bare-airframe helicopter without controller assistance and is the backup for the experimental system. The experimental system provides the high flexibility required for research activities and allows for feedback control assessment through flight testing.

Model-based control is used on the ACT/FHS [2, 3]. This control scheme has to ensure that certain control assistance ease helicopter flight so that pilot workload is reduced. One highly challenging application and research topic of this control assistance is an in-flight simulation that will be pursued with the DLR project Assisted Low Level Flight Using In-Flight Simulation Capability (ALL-in-Flight). That is, the pilot would believe that s/he is flying another helicopter. A second application is directed to Handling Qualities and intends easy flying. The respective model can be directly defined by using ADS33 [4] or user-defined so that it is comparable to driving a car [5]. All these goals require highly performant feedback control which is crucial for state tracking of the arbitrarily defined reference models. The challenge addressed in this paper is the mismatch between simulated and measured closed-loop behavior. The proposed solution is a tailored framework that describes the plant's model as a combination of physics-based and generic models used for feedback control design. The paper continues with the state of the art in section 2 and shows then the aforementioned framework as an overview in section 3 followed by the detailed descriptions of the framework in sections 4-7. The paper finally shows flight test examples in section 8 and is concluded in 9. Examples company the sections and represent qualitatively the observations made in flight tests with the ACT/FHS.



Figure 1: DLR's research helicopter ACT/FHS

2. STATE OF THE ART

The mismatches between the helicopter simulation and the respective measurements drive the continuous improvement of nonlinear simulation programs such as HOST (Helicopter Overall Simulation Tool, [6]) or DLR's SimH [7]. The effort is worthwhile as the nonlinear model serves with their numerically linearized models as feedback design platform and with their real-time capability as a testing platform for future flight tests, and in industrial application as training device for pilots.

For feedback control design in helicopter applications, linear models are state of the art [8, 9, 10]. These models are derived by numerically linearizing nonlinear helicopter programs such as in reference [9] or by system identification as used in references [10, 11]. The identification technique is an empirical method that maps parameters of a model such that measured outputs are described with certain inputs. The modeling accuracy typically depends on the order of the model and should meet specific requirements so that feedback control design is possible. Linear models derived by system identification are used for the feedback control design in references [12, 13] for instance. The usage of numerically linearized models from HOST for example are documented in reference [14].

What if the linear model is not accurate and the expected closed-loop behavior cannot be observed in real flight? To improve the closed-loop behavior, the design may either focus more on the controller design or more on the modeling. The approach chosen here is to describe the model uncertainties to ease the design of a high-bandwidth control while still classical feedback control schemes can be used.

Feedback design often uses linear models and uncertainties may also arise through local nonlinear remnants [9]. Appending known nonlinear terms to the linear point model promises at least a broader validity and may also respect certain nonlinear remnants. References [15, 16] show a feasible approach applied to the ATHeS research rotor-

craft. Both references show the spline-based interpolation of linear matrices in combination with nonlinear terms such as altitude, gravity, and inertia. Tischler and Zivan [9, 17] additionally use trim curves to set up the stitched model. Different linear point models of a Bell 206 (derived by system identification) are interpolated and the respective pilot ratings show a good simulation fidelity. Reference [18] applied a stitching technique to identification results of the ACT/FHS and showed a good quantitative match for the overall flight envelope. Reference [19] recently shows impressively (for the light business jet Cessna Citation CJ1) that the stitching technique features not only the interpolation but also the extrapolation which requires only few linear point models. The effect of a changing mass and altitude for instance is extrapolated with prescribed relationships. The pilot ratings of the full envelope Cessna simulation underline the high-fidelity simulation and indicate that the stitching may serve as real-time simulation.

However, mismatches between simulated and measured output can still remain. The predictive accuracy can be assessed in the frequency domain with maximum unnoticeable added dynamics (MUAD) [20, 21] which indicate frequencies that show relevant model mismatches. Additional models for the outputs may be derived, so that the simulated response predicts the measurements. The more outputs the model has, the more complex it becomes to achieve a perfect consistency. Another strategy is to analyze the inputs and ask for residual inputs that have to be added to predict the measurements. Inverse simulation is one possible method to calculate these residual inputs and is introduced in references [22, 23, 24]. The subsequent development of a non physics-based model for these residual control is introduced in reference [25]. As a positive consequence, the consistency of the outputs is still ensured.

Even high-fidelity models for helicopters may still fail in predicting the closed-loop response. A prominent example is the so-called air resonance that is not well-predicted for the ACT/FHS with neither nonlinear helicopter models nor linear models derived by system identification. This result motivates the application of partial closed-loop control in real flight as a technique for model validation. Partial closed-loop control for the ACT/FHS means that only one feedback axis is active. Feeding back measurements to a single axis still ensures uncorrelated inputs which are quite often a pre-requisite for system identification. This method was already successfully applied for the roll axis in references [13, 26, 27]. The technique is adopted from validation of nonlinear simulation tools where numerical integration of certain subsystems is broken and measurements are used instead [28]. It is applied for example for an engine model of the Bo-105 in reference [7] and for the Fenestron model of the EC135 in reference [29].

This paper shows a feasible approach to combine model stitching, inverse simulation, and partial closed-loop to ob-

tain a full flight envelope model with uncertainties. The goal is to provide a model of the ACT/FHS for high-performant feedback control design.

3. STEPS TO OBTAIN THE MODEL OF THE PLANT: AN OVERVIEW

Consider a linear model describing the helicopter motion without controller assistance at a certain operating point. Assume further that the linear model has a lack of modeling accuracy. Reference [30] proposes different structures for the uncertainties of a linear model. Two of these structures are presented in the block diagram of figure 2. These uncertainties may be expressed with parametric and structured systems so that the overall transfer function matches the measurements at least for the deterministic part. Remaining stochastic uncertainties may also exist but are not addressed in this paper.

The linear models are derived by system identification and are presented in section 4. In accordance with figure 2, a three-step approach is chosen to obtain the uncertainties together with the full envelope model:

- **The Full Flight Envelope Model:**

The linear point models are stitched together such that airspeed dependent maneuvering flight is possible [17, 18]. Known nonlinearities such as trim curves and gravity are taken into account to arrive at a full envelope simulation. Section 5 shows the application to models of the ACT/FHS.

- **Inverse Simulation to Obtain Input Uncertainties:**

By means of inverse simulation, the second step facilitates a detailed analysis of the controls that are necessary to obtain the measured response, [24, 25]. The comparison between inverse-simulated and measured controls finally allows for the modeling of the input uncertainty. With this technique, section 6 shows that the modeling quality can be improved for the ACT/FHS without feedback control.

- **Partial Closed-Loop for Additive Uncertainties:**

The third step features the analysis of the model for its application to feedback control design. The model is simulated with feedback and the closed-loop re-

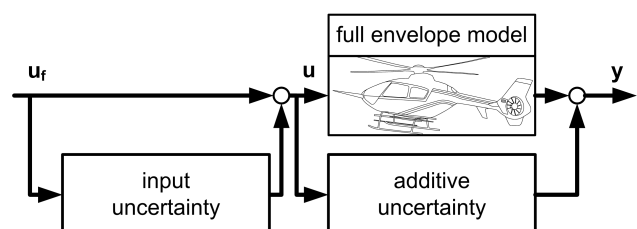


Figure 2: Uncertainties to improve the plant's model for flight control design

sponses between simulation and measurements are compared, [13, 26]. The feedback is only applied to a single control axis (and is called partial closed-loop) to avoid correlation between multiple inputs. Section 7 finally shows how to determine the additive uncertainty so that the model of the plant (see figure 2) is prepared for its application to feedback control design.

4. THE ORIGINAL MODEL DERIVED BY SYSTEM IDENTIFICATION

System identification is based on a physical model with certain parameters. For the ACT/FHS, five operating points are chosen by experience dependent on airspeed from hover to 120 knot in steps of 30 knot. It is believed that the five point models cover the strongly varying flight dynamics from hover to fast forward flight. Each linear model respects frequencies up to 20 rad/s and degrees of freedom depicted in figure 3, namely the body-fixed velocities (u , v , and w), angular rates (p , q , and r), flapping (a and b), regressive lead-lag (x_{ll} , and y_{ll}), and mean inflow (v). Flapping and mean inflow are expressed implicitly by the angular acceleration \dot{p} , \dot{q} and vertical acceleration \dot{w} , respectively [8, 18]. The linear model has the form of a state space model [30] with inputs $\Delta \mathbf{u} \in \mathbb{R}^m$, outputs $\Delta \mathbf{y} \in \mathbb{R}^l$, and states $\Delta \mathbf{x} \in \mathbb{R}^n$. The state and output equations of the system are:

$$(1) \quad \begin{aligned} \Delta \dot{\mathbf{x}} &= \mathbf{A}_{\xi_{PID}} \Delta \mathbf{x} + \mathbf{B}_{\xi_{PID}} \Delta \mathbf{u} \\ \Delta \mathbf{y} &= \mathbf{C}_{\xi_{PID}} \Delta \mathbf{x} + \mathbf{D}_{\xi_{PID}} \Delta \mathbf{u} \end{aligned}$$

with the system matrix $\mathbf{A}_{\xi_{PID}}$, the input matrix $\mathbf{B}_{\xi_{PID}}$, the output matrix $\mathbf{C}_{\xi_{PID}}$ and the feedthrough matrix $\mathbf{D}_{\xi_{PID}}$. The index ξ_{PID} denotes the airspeed at the operating point which may be hover, 30 knot, \dots , 120 knot. The matrix $\mathbf{A}_{60 \text{ knot}}$ for instance is the system matrix obtained for 60 knot forward flight. The inputs of the system are the four controls of the helicopter that are longitudinal δ_x , lateral δ_y , pedal δ_p , and collective δ_0 control.

$$(2) \quad \Delta \mathbf{u} = (\Delta \delta_x, \Delta \delta_y, \Delta \delta_p, \Delta \delta_0)^T$$

The states comprise the fixed-body with its velocities, rates,

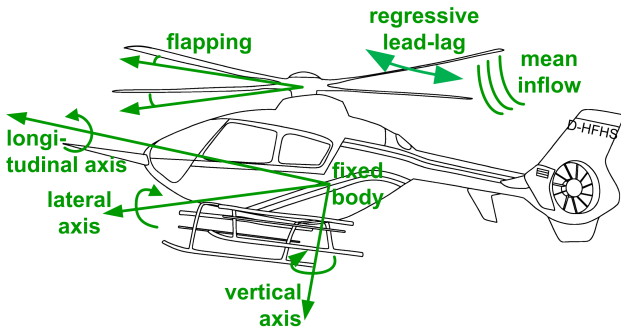


Figure 3: Degrees of freedom to model the flight dynamics of the ACT/FHS

and attitudes, the implicit flapping as well as lead-lag of the main rotor blades, and the mean inflow as non-physical state w_h [18]:

$$(3) \quad \Delta \mathbf{x} = (\Delta u, \Delta v, \Delta w, \Delta p, \Delta q, \Delta r, \Delta w_h, \Delta \dot{p}, \Delta \dot{q}, \Delta \phi, \Delta \theta, \Delta x_{ll,1}, \Delta x_{ll,2}, \Delta y_{ll,1}, \Delta y_{ll,2})^T$$

The outputs are chosen such that corresponding measurements are available:

$$(4) \quad \Delta \mathbf{y} = (\Delta u, \Delta v, \Delta w, \Delta p, \Delta q, \Delta r, \Delta \phi, \Delta \theta, \Delta a_x, \Delta a_y, \Delta a_z, \Delta \dot{p}, \Delta \dot{q}, \Delta \dot{r})^T$$

The accuracy of these models is typically assessed in the time-domain with the cost function proposed in reference [9]. To express the model quality, the following variables:

$$(5) \quad \tilde{\mathbf{y}} = (\alpha, \beta, p, q, r, a_x, a_y, a_z, \phi, \theta)$$

are used to calculate the root mean square error (RMS) of a single run:

$$(6) \quad J_{RMS} = \sqrt{\frac{1}{n_{outputs} \cdot n_{samples}} \sum_{k=0}^{n_{samples}} J_k}$$

with: $J_k = (\tilde{\mathbf{y}}_{meas,k} - \tilde{\mathbf{y}}_k) \mathbf{Q} (\tilde{\mathbf{y}}_{meas,k} - \tilde{\mathbf{y}}_k)^T$

The cost is normalized by the number of outputs $n_{outputs}$ (i.e. ten in equation (5)) and by the number of samples $n_{samples}$. The output errors are weighted with \mathbf{Q} such that the linear motion variables are given in ft, %s, \dots and the rotational ones in $^\circ$, %s, \dots . Adequate accuracy for rotorcraft modeling is achieved [9] when

$$1.0 \leq J_{RMS} \leq 2.0$$

For smaller values of J_{RMS} , the modeling quality can be considered to be good. This validation is performed for all point models. For validation purposes, 3211- and 2311-multistep inputs are used. The length of each run varies between nine and twelve seconds. The number of analyzed response data sets varies for each operating point from 9 (120 knot) to 24 runs (30 knot). The RMS is calculated for each run individually and then plotted by means of boxplots as shown in figure 4. An individual run for the longitudinal 3211-multistep input is shown in figure 5.

The boxplot comprises the median as red line, the box with 50% of the data, the whisker with maximum three-times of the box length, and the outliers marked as circles. Each run is assigned to a specific operating point which gives the first diagram in figure 4. The second diagram is obtained through assigning the control axis that features the multi-step input. The third diagram shows a single output (i.e. roll, pitch, yaw, and climb rate) which is a single element of the output vector of equation (5).

Most of the data show adequate modeling quality as depicted with the median of the airspeed-dependent box plots.

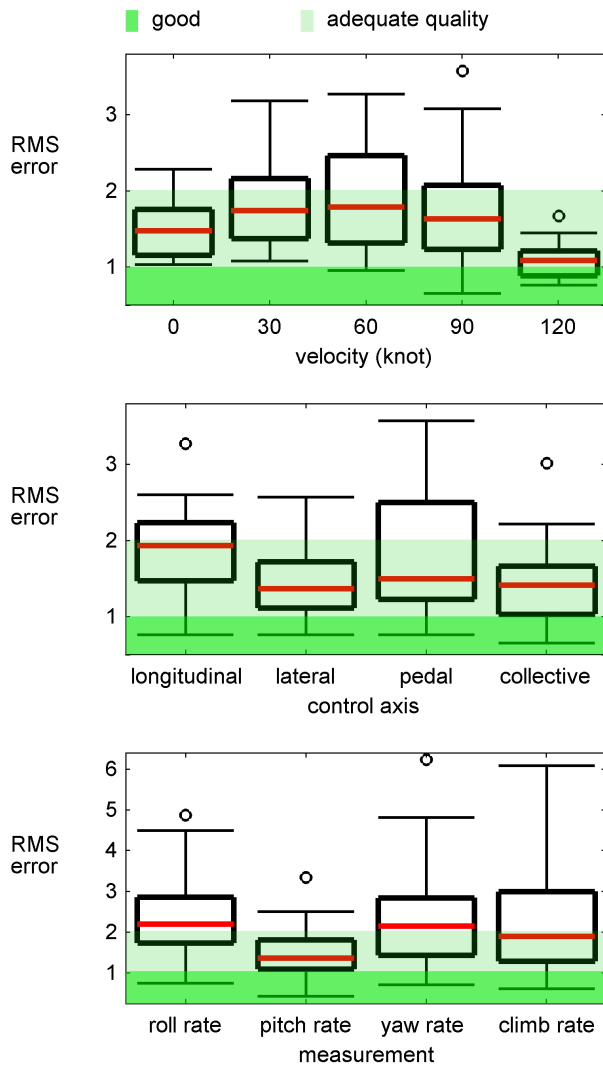


Figure 4: Root mean square error of all operating point models depending on velocity, control axis, and measured variable

The model for 120knot shows the best accuracy but is still adequate. The point models for 30knot, 60knot, and 90knot show slightly higher RMS values when compared to the hover case which is adequate for the majority of cases. The 30knot model shows reasonable results even though the ACT/FHS is trimmed either at 25knot or at 35knot which results in challenging conditions for system identification. Lateral and collective control inputs show adequate quality in most cases whereas longitudinal and pedal control inputs are characterized by modeling deficiencies. The on-axis as well as coupling to the pitch rate is predicted well whereas the simulation of roll, yaw, and climb rate should be improved and suffers from the highly coupled dynamical behavior of the ACT/FHS.

A single measurement is shown in figure 5. As expected by the RMS, the response of the pitch acceleration is covered well whereas higher frequencies with approximately 35 rad/s

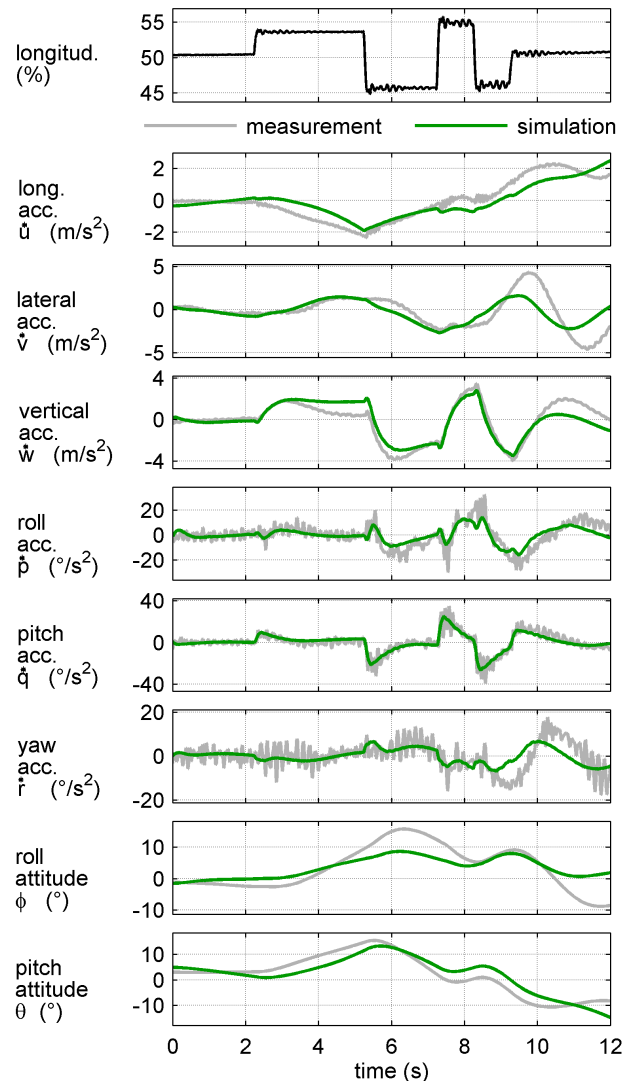


Figure 5: Comparison in time domain between measured or reconstructed (grey) and simulated (green) values for the multi-step input at 60knot forward flight

are not covered. The roll and yaw acceleration are predicted adequately but show deficiencies for smaller frequencies, e.g. roll at $t \approx 6 \text{ s}$, and yaw at $t \approx 10 \text{ s}$. The linear accelerations are predicted adequately, too, whereas lateral acceleration needs to be improved for smaller frequencies. Especially small frequencies are respected by the RMS so that the results depicted in time domain can be empirically translated into a corresponding RMS value.

It is believed, that the existing modeling deficiencies originate from the absence of both engine and Fenestron models. For 120knot, the influence of the engine on the system's response is small, so that the RMS value is also small when compared to other airspeed-dependent operating points. Additionally, the RMS for pedal inputs varies strongly which may be caused by the missing Fenestron model. Respecting both, the Fenestron and engine, may further improve the modeling quality. However, physics-

based modeling is almost always difficult so that the mismatch between simulation and measurement will be described by generic models. The linear models can be enhanced by nonlinear terms and uncertainties (see figure 2) which will be presented in the following based on ACT/FHS flight test data.

5. THE FULL FLIGHT ENVELOPE MODEL

Basically, the single operating point models have a limited validity. If airspeed changes, another discrete model may be needed. The colored curves in figure 6 show this effect for different airspeeds. The modeling quality is significantly reduced if a specific operating point model is used at a non intended airspeed. The blue curve for instance comprises the point model derived for 60knot forward flight and this model is used to simulate the flight test data obtained at all operating points. The dots represent the median (e.g. red line in figure 4) as obtained through equation (6). In all cases, the point model works best when used for the intended operating point. The so-called model stitching technique [9, 17, 18] interpolates the point models smoothly so that the helicopter dynamics are adapted to airspeed. The median of the RMS value of the stitched model is shown with the black curve in figure 6 and clearly indicates that this model covers the flight envelope. The following section summarizes the results obtained in stitching identified linear models of the ACT/FHS.

Method. The stitching technique requires flight test data for the dynamical and stationary behavior. For this purpose flight tests should also cover trim analysis at different conditions such as different airspeeds, quartering flight, and altitudes. Trim data for the ACT/FHS at different airspeeds are depicted in figure 7 for the attitudes and controls. Roll attitude shows some outliers which may arise through trimming the helicopter either with slight angle of sideslip or without.

Consider a linear system such as equation (1) given at an operating point ξ_{PID} . For this model, only the state equation is taken into account as the states already have a physical meaning that corresponds to the measured outputs \mathbf{y} . All elements of the state equation (matrices and constants at the operating point) are now considered to depend on the trim condition. The trim variable ξ controls the selection of the trim condition smoothly. With this, the state equation of the stitched model is

$$(7) \quad \begin{aligned} \Delta \dot{\mathbf{x}} &= \mathbf{A}(\xi_f) (\mathbf{x} - \mathbf{x}_{t,f}) + \mathbf{B}(\xi_f) (\mathbf{u} - \mathbf{u}_t(\xi)) + \\ &\quad \mathbf{f}(\mathbf{x}, \mathbf{u}) - \mathbf{f}(\mathbf{x}_t(\xi), \mathbf{u}_t(\xi)) \\ \text{with: } \xi &= \sqrt{u_b^2 + v_b^2 + w_b^2} \\ \dot{\xi}_f &= -1/T_1 \xi_f + 1/T_1 \xi, \xi_f(0) = \xi_{PID} \\ \mathbf{x}_{t,f} &= \mathbf{x}_t(\xi_f) \\ \mathbf{x}(t=0) &= \mathbf{x}_t(\xi_{PID}), \mathbf{u}(t=0) = \mathbf{u}_t(\xi_{PID}) \end{aligned}$$

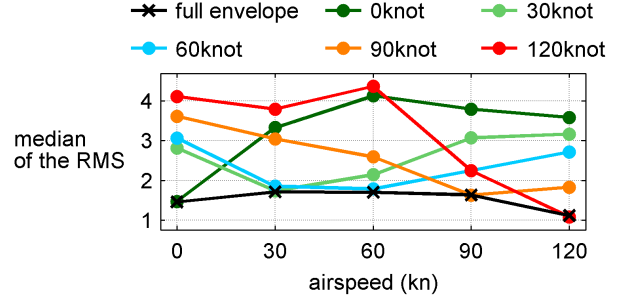


Figure 6: Median of the RMS value (equation (6)) of the point models at each airspeed (colored curves) and the RMS of the stitched model (black curve)

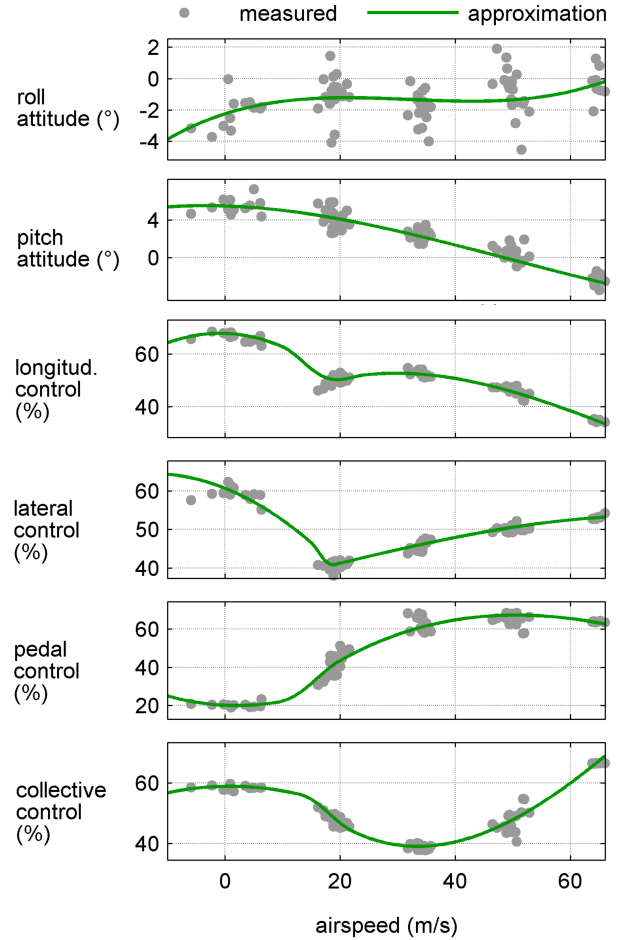


Figure 7: Trim variables depending on airspeed

The input vector $\Delta \mathbf{u} = \mathbf{u} - \mathbf{u}_{t,\xi_{PID}}$ for instance is now a function of the trim variable and leads to $\mathbf{u} - \mathbf{u}_t(\xi)$. The term $\mathbf{u}_t(\xi)$ respects the trim controls as depicted with the green curves in figure 7. Additionally, known nonlinear terms such as gravity or inertia are respected with the nonlinear vector $\mathbf{f}(\mathbf{x}, \mathbf{u})$. The trim variable ξ is filtered with a large time constant T_1 to obtain ξ_f which is then used to calculate the filtered trim states $\mathbf{x}_{t,f}$. The filtered trim states comprise the roll and pitch attitude as depicted with the green curves in figure 7 and also respect the trim velocities. The

trim variable is the airspeed which is calculated by means of the three body-fixed velocity components u , v , and w . The body-fixed velocities are bounded so that a 30 knot side-ward flight with zero forward and vertical speed do not lead to the selection of the 30 knot operating point model. Details on the bounds u_b , v_b , and w_b are documented in reference [18]. The linearized equation (7) at a specific operating point ξ_{PID} should exactly be the same as the originally linear model derived by system identification equation (1). With this assumption, the linear matrices $\mathbf{A}(\xi_f)$ and $\mathbf{B}(\xi_f)$ are calculated at the predefined operating points and are then interpolated with respect to airspeed.

Application to ACT/FHS data. The stitched model allows for maneuvering flight. Dependent on airspeed, the appropriate trim controls and states together with system and input matrix are used. The linearized equation (7) provides the eigenvalues and their transition between the originally five operating points. Figure 8 shows the respective eigenvalues. The path of the eigenvalues looks original and motivates the application as model for the maneuvering flight. The main achievement of the stitching (for the most recent system identification results obtained for the ACT/FHS) is, that the helicopter dynamics are automatically selected depending on airspeed. The RMS error between stitched and point model is similar for each operating point as shown in figure 6. Maneuvering flight such as acceleration and deceleration for example can be simulated with the stitched model.

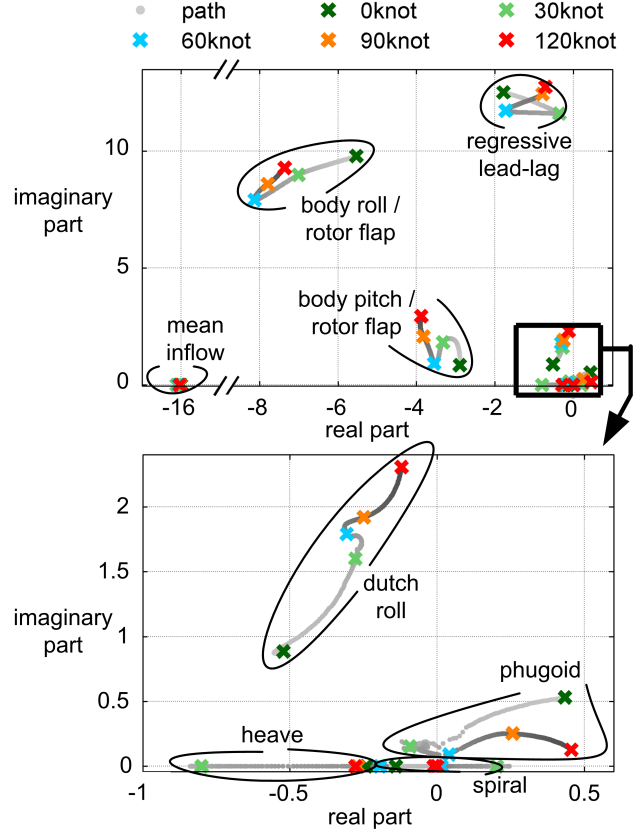


Figure 8: Eigenvalues and their transition between the operating points

6. INVERSE SIMULATION TO OBTAIN INPUT UNCERTAINTIES

Originally, inverse simulation is a tool for model validation [22, 24]. However, this tool can also be used to extend the physics-based model by certain generic ones which give the input uncertainty in figure 2.

Method. The inverse simulation procedure is sketched in figure 9. This simulation technique computes control inputs $\mathbf{u}_{i,s}$ such that the measured outputs are obtained with these controls for a given model [23, 24]. The comparison between the inverse simulated and original inputs helps analyzing modeling deficiencies. Inverse simulation translates the modeling errors such that these can be observed for the inputs. It is stressed, that the classical simulation shows the differences and modeling errors for the measured outputs as shown with the time domain result in figure 5. Given a linear system such as equation (1), the partitioned state space model becomes

$$(8) \quad \begin{pmatrix} \Delta \dot{\mathbf{x}}_{s,1} \\ \Delta \dot{\mathbf{x}}_{s,2} \end{pmatrix} = \begin{bmatrix} \mathbf{A}_{11} & \mathbf{A}_{12} \\ \mathbf{A}_{21} & \mathbf{A}_{22} \end{bmatrix} \begin{pmatrix} \Delta \mathbf{x}_{s,1} \\ \Delta \mathbf{x}_{s,2} \end{pmatrix} + \begin{bmatrix} \mathbf{B}_1 \\ \mathbf{B}_2 \end{bmatrix} \Delta \mathbf{u}$$

$$\Delta \mathbf{x}_{s,1} = [\mathbf{I} \quad \mathbf{0}] \begin{pmatrix} \Delta \mathbf{x}_{s,1} \\ \Delta \mathbf{x}_{s,2} \end{pmatrix}$$

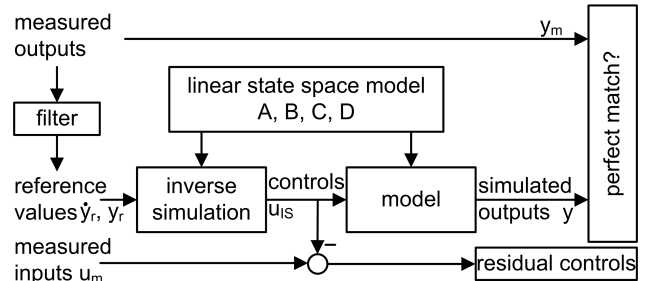


Figure 9: Inverse simulation to compute residual controls

The outputs $\Delta \mathbf{x}_{s,1}$ are user-defined, have (typically) the same dimension as the control inputs, and are linearly independent from one another. An important requirement is that the feedthrough matrix must be zero for the output variables $\Delta \mathbf{x}_{s,1}$. The task for the inverse simulation is to compute the controls $\Delta \mathbf{u}_{i,s}$ such that the values $\Delta \mathbf{x}_{s,1}$ exactly match the corresponding measurements \mathbf{y}_m . For the application to ACT/FHS models, typical outputs are pitch acceleration \dot{q} , roll acceleration \dot{p} , yaw rate r , and climb rate w with the respective inputs longitudinal δ_x , lateral δ_y , pedal δ_p , and collective δ_0 . If the matrix $[\mathbf{A}_{22} - \mathbf{B}_2 \mathbf{B}_1^{-1} \mathbf{A}_{12}]$ is stable, then the inverse simulated controls $\Delta \mathbf{u}_{i,s}$ are obtained through (see references [25, 31]):

$$\begin{aligned}
\Delta \dot{\mathbf{x}}_{s,2} &= \mathbf{A}^* \Delta \mathbf{x}_{s,2} + \mathbf{B}^* \begin{pmatrix} \Delta \dot{\mathbf{y}}_r \\ \Delta \mathbf{y}_r \end{pmatrix} + \Delta \dot{\mathbf{x}}_{i,2} \\
\Delta \mathbf{u}_{is} &= \mathbf{C}^* \Delta \mathbf{x}_{s,2} + \mathbf{D}^* \begin{pmatrix} \Delta \dot{\mathbf{y}}_r \\ \Delta \mathbf{y}_r \end{pmatrix} \\
\text{with: } \mathbf{A}^* &= [\mathbf{A}_{22} - \mathbf{B}_2 \mathbf{B}_1^{-1} \mathbf{A}_{12}] \\
\mathbf{B}^* &= [\mathbf{B}_2 \mathbf{B}_1^{-1} \quad \mathbf{A}_{21} - \mathbf{B}_2 \mathbf{B}_1^{-1} \mathbf{A}_{11}] \\
\mathbf{C}^* &= -\mathbf{B}_1^{-1} \mathbf{A}_{12} \\
\mathbf{D}^* &= [\mathbf{B}_1^{-1} \quad -\mathbf{B}_1^{-1} \mathbf{A}_{11}] \\
\Delta \dot{\mathbf{x}}_{i,2} &= -\mathbf{B}^* \begin{pmatrix} \Delta \dot{\mathbf{y}}_r(0) \\ \Delta \mathbf{y}_r(0) \end{pmatrix}, \quad \Delta \mathbf{x}_{s,2}(0) = \mathbf{0}
\end{aligned}
\tag{9}$$

Equation (9) is initialized such that all derivatives $\Delta \dot{\mathbf{x}}_{s,2}$ are zero at $t = 0$. The inverse simulation uses reference values $\Delta \mathbf{y}_r$ and their derivatives $\Delta \dot{\mathbf{y}}_r$, which require corresponding measurements \mathbf{y}_m and $\dot{\mathbf{y}}_m$, respectively. Dependent on the level of noise, the inverse simulated controls will be noisy as well which is distracting for the further analysis. The flight test data \mathbf{y}_m are thus filtered such that measuring noise is reduced and the reference values \mathbf{y}_r are consistent to one another. The influence of disturbances such as wind and uncertain trim conditions is estimated and is detailed in reference [25].

The inverse simulated controls are compared to the measured controls. For the purpose of flight control design, especially the analysis in frequency domain is of interest. Thus the frequency response of the residual controls due to the measured inputs is calculated. The Laplace representation with s being the Laplace variable is:

$$\mathbf{G}_{is,m} = \frac{\mathbf{U}_{is}(s) - \mathbf{U}_m(s)}{\mathbf{U}_m(s)}
\tag{10}$$

If the frequency representation $\mathbf{G}_{is,m}$ is mostly deterministic over frequency, the input uncertainty Δ_m may model the missing or not considered dynamical behavior. Inverse simulation thus assists the analysis of the bare-airframe helicopter.

Example. The approximated on-axis pitch motion of the ACT/FHS at 60 knot is given by

$$\begin{aligned}
\begin{pmatrix} \Delta \dot{\theta} \\ \Delta \dot{q} \\ \Delta \ddot{q} \end{pmatrix} &= \begin{bmatrix} 0 & 1 & 0 \\ 0 & 0 & 1 \\ 0 & M_q & M_{\dot{q}} \end{bmatrix} \begin{pmatrix} \Delta \theta \\ \Delta q \\ \Delta \dot{q} \end{pmatrix} + \begin{pmatrix} 0 \\ 0 \\ M_{\delta_x} \end{pmatrix} \Delta \delta_x \\
\Delta \dot{q}_m &= [0 \quad 0 \quad 1] \begin{pmatrix} \Delta \theta \\ \Delta q \\ \Delta \dot{q} \end{pmatrix} \\
\text{with: } &(\Delta \theta(0) \quad \Delta q(0) \quad \Delta \dot{q}(0))^T = \mathbf{0}, \\
&\Delta \delta_x(0) = 0
\end{aligned}
\tag{11}$$

The numerical values are

$$M_q = -13 \text{ } 1/\text{s}^2, \quad M_{\dot{q}} = -7 \text{ } 1/\text{s}, \quad M_{\delta_x} = 0.75 \text{ rad}/\% \text{ s}^3
\tag{12}$$

The output $\Delta \dot{q}_m$ is selected to obtain the match between simulation and measurement, i.e. $\Delta \mathbf{x}_{s,1} = \Delta \dot{q}_m$ in equation (8). Inverse simulation requires this output together with its derivative so that $\Delta \dot{q}_m$ is filtered and integrated again to obtain the desired consistent reference values (i.e. \dot{q}_r, \ddot{q}_r) for inverse simulation.

For the purpose of this example, it is assumed that system identification estimates $\tilde{M}_{\dot{q}} = -9$. Thus, the inverse simulated control is computed under this erroneous estimation.

$$\begin{aligned}
\begin{pmatrix} \Delta \dot{\theta}_s \\ \Delta \dot{q}_s \end{pmatrix} &= \begin{bmatrix} 0 & 1 \\ 0 & 0 \end{bmatrix} \begin{pmatrix} \Delta \theta_s \\ \Delta q_s \end{pmatrix} + \begin{bmatrix} 0 & 0 \\ 0 & 1 \end{bmatrix} \begin{pmatrix} \Delta \ddot{q}_r \\ \Delta \dot{q}_r \end{pmatrix} \\
\Delta \delta_{x,is} &= -M_q/M_{\delta_x} \Delta q_s + [1 \quad \tilde{M}_{\dot{q}}/M_{\delta_x}] \begin{pmatrix} \Delta \ddot{q}_r \\ \Delta \dot{q}_r \end{pmatrix}
\end{aligned}
\tag{13}$$

Inserting the control law equation (13) into equation (11) (use $\Delta \delta_{x,is}$ instead of $\Delta \delta_x$) yields the simulated pitch acceleration that matches the respective reference value, figure 10. Due to the erroneous estimation of the stability derivative $\tilde{M}_{\dot{q}}$, the measured and inverse simulated longitudinal controls are different. The frequency response is calculated using equation (10). Figure 11 shows the response of the residual control $\Delta \delta_{x,is} - \Delta \delta_x$ due to the original control $\Delta \delta_x$. The respective model is obtained by estimation methods that are implemented in Fitlab [32, 33]. In this example, the model Δ_m can be given analytically by:

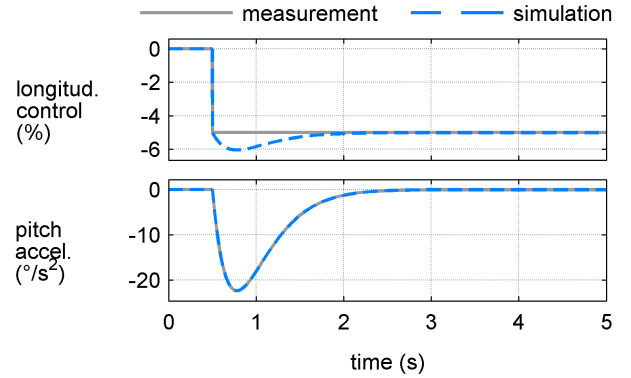


Figure 10: Example for the inverse simulation of pitch axis

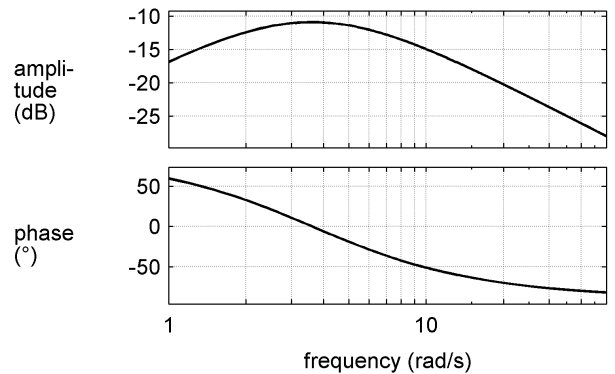


Figure 11: Input uncertainty of the pitch axis example

$$(14) \quad \Delta_m = \frac{(M_{\dot{q}} - \tilde{M}_{\dot{q}})s^2}{s^3 - M_{\dot{q}}s^2 - M_q s}$$

If the model Δ_m is used as input uncertainty as presented in figure 2, then the modeling quality is significantly improved. Although this example only demonstrates how to handle parameter uncertainties of a linear system, the same procedure can be applied if certain degrees of freedom are missing. Finally, the example underlines that inverse simulation is a promising technique for estimating a structured input uncertainty and is a reliable tool for model validation.

Application to ACT/FHS data. Each point model is analyzed for the respective flight test data by means of inverse simulation. Then, the inverse calculated controls are compared with the measured controls of the ACT/FHS. As an example, flight test data with collective input are used. Especially the inverse simulated pedal axis shows dominant amplitudes which are needed to obtain the measured helicopter motion. The respective frequency response of the additional pedal input due to measured collective control is shown in figure 12 (grey curves) and is computed adapting equation (10) which gives:

$$(15) \quad \mathbf{G}_{is,m,p0} = \frac{\delta_{is,p}(s) - \delta_{m,p}(s)}{\delta_{m,0}(s)}$$

Figure 12 collects the computed frequency responses for all test data from hover to 120 knot. The larger the amplitudes of the frequency response, the larger the modeling uncertainties are. The value 0 dB for instance means that the collective is directly added on the pedal axis. Frequencies around $4 \text{ rad/s} \leq \omega \leq 16 \text{ rad/s}$ are not covered that well by the original linear model. It is believed that an additional engine model within the system identification would improve modeling quality and reduce the inverse simulated pedal input within the aforementioned frequency range. Additionally, the resonance phenomenon at approximately $\omega = 35 \text{ rad/s}$ is not covered by the original model derived by system identification and accumulates several effects such as structural oscillations of the tailboom and coning. This effect is observed for all other control axes, while these are almost only characterized by this resonance.

For all control axes, a model approximates the frequency response. The red curve in figure 12 represents the model that calculates the residual pedal due to collective control. The modeling procedure is repeated for all other control axes so that, finally, the input uncertainty is obtained. With this, missing or not considered dynamical effects of the original point models are respected by means of a combination of physics-based model and generic input uncertainty.

Figure 13 shows the time domain response at 60 knot due to longitudinal input (compare figure 5). Again, the pure point model derived by system identification is depicted with the

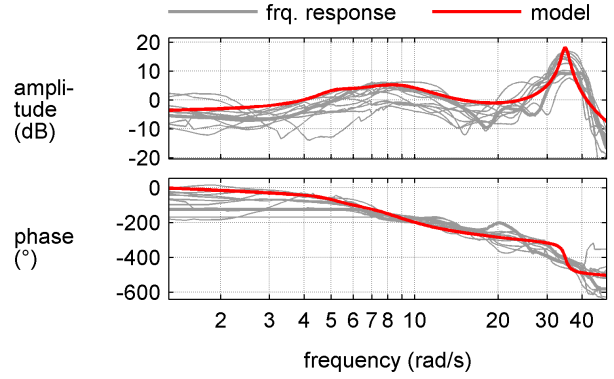


Figure 12: Input uncertainty for ACT/FHS data, residual pedal due to collective control

green curves. In comparison, the same point model is simulated together with the input uncertainty (blue curves). With input uncertainty, the match is improved. Especially, lateral velocity, roll acceleration, and yaw acceleration benefit from the modeled input uncertainty.

The advantage of using only one model for the input uncertainty for all velocities (aside from time savings) is that it can be easily attached to the stitched model. There is no interpolation dependent on airspeed needed. The drawback is that the overall model cannot be improved as much as possible. However, the improved prediction capability is highly motivating, as the modeling deficiencies have been there for years. Especially flight control design benefits from the model improvement. If further and more detailed modeling is needed for feedback design, the technique presented above just needs to be applied to each operating point but, then, the models have to be interpolated.

7. PARTIAL CLOSED-LOOP TO OBTAIN ADDITIVE UNCERTAINTIES

System identification is based on flight test data whereas small amplitudes and rates are used to excite the ACT/FHS without feedback. The resulting models cover the flight-dynamical behavior of the ACT/FHS and should allow for feedback design. For the roll axis, the preliminary feedback control design leads to an unexpected roll oscillation in flight tests with the ACT/FHS [13, 26]. This result motivates partial closed-loop as a method to identify additional uncertainties (see figure 2), so that the closed-loop behavior is predicted by the model.

Method. Partial closed-loop consists of only one feedback axis while the remaining axes have no feedback control. In this way, correlation is still small which is often a prerequisite for system identification [8]. In flight tests, measurements are fed back to a single axis. The remaining axes are controlled by the pilot directly. In simulation, the recorded

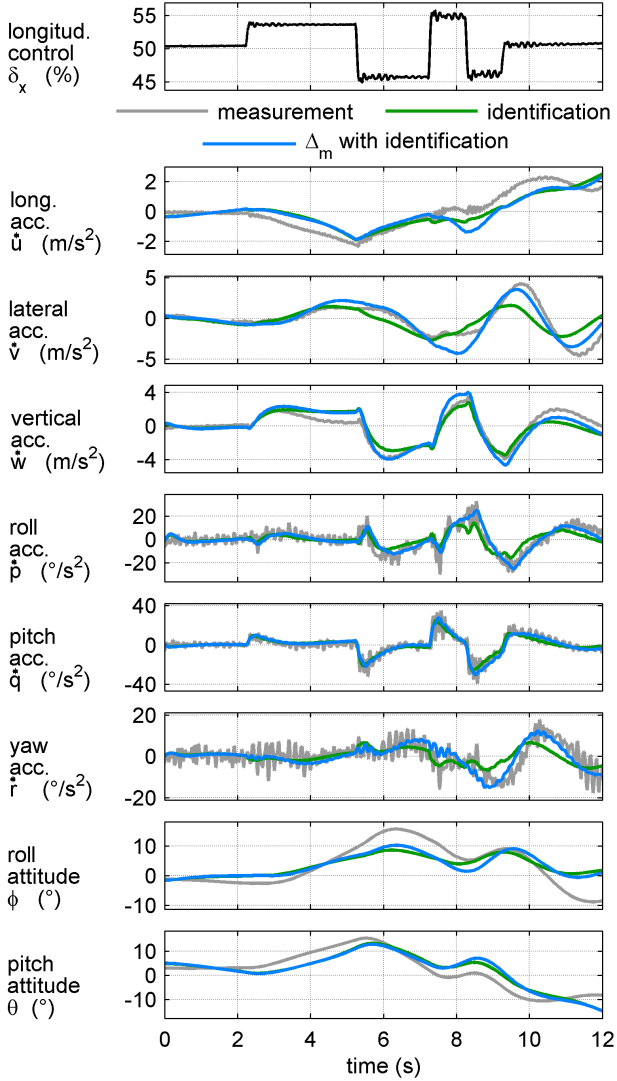


Figure 13: Predictive Capability for 60knot forward flight, measurements (grey), point model (green), and point model with input uncertainty (blue)

data of the remaining axes are used as direct input for the model and the feedback axis is simulated. The technique was first applied to the roll axis to predict the so-called air resonance which is an oscillating roll motion. Reference [34] shows how to adapt point models as well as the non-linear helicopter simulation to predict air resonance. More specifically, measured rates such as roll, pitch, yaw, and climb rate are used for feedback on the respective control axis. The measured response is compared with the simulated one and certain parameters of the additive uncertainty are optimized until the simulated response matches the measured one. The additional uncertainty is simply set up as a state space model with the same dimension as the point model. The block diagram in figure 14 summarizes the procedure for the lateral axis.

The point model with additional uncertainty is set up with the

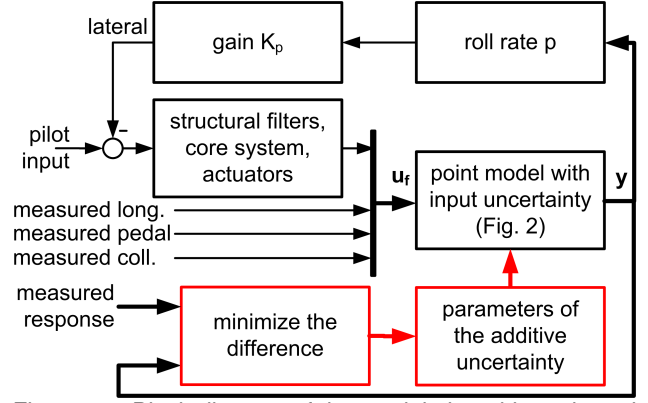


Figure 14: Block diagram of the partial closed-loop, lateral control is activated

additional system matrix $\mathbf{A}_{a,\xi_{PID}}$ and input matrix $\mathbf{B}_{a,\xi_{PID}}$. For each operating point, specific additive matrices $\mathbf{A}_{a,\xi_{PID}}$ and $\mathbf{B}_{a,\xi_{PID}}$ are used.

$$\begin{aligned}
 \Delta \dot{\mathbf{x}} &= (\mathbf{A}_{\xi_{PID}} + \mathbf{A}_{a,\xi_{PID}}) \Delta \mathbf{x} \\
 &\quad + (\mathbf{B}_{\xi_{PID}} + \mathbf{B}_{a,\xi_{PID}}) \Delta \mathbf{u} \\
 \Delta \mathbf{y} &= \mathbf{C}_{\xi_{PID}} \Delta \mathbf{x} + \mathbf{D}_{\xi_{PID}} \Delta \mathbf{u} \\
 \Delta \mathbf{u} &= \Delta_m \Delta \mathbf{u}_f + \Delta \mathbf{u}_f
 \end{aligned}
 \tag{16}$$

The minimization of the error between simulation and measurement is conducted as follows

$$\min_{\substack{\mathbf{A}_{a,\xi_{PID}} \\ \mathbf{B}_{a,\xi_{PID}}}} \left((\Delta \mathbf{y} - \Delta \mathbf{y}_m)^T \mathbf{C}_a^T \mathbf{C}_a (\Delta \mathbf{y} - \Delta \mathbf{y}_m) \right)
 \tag{17}$$

The output matrix \mathbf{C}_a selects the output variables which are a_x , a_y , a_z , \dot{p} , \dot{q} , and \dot{r} .

Application to ACT/FHS data. Flight test data are used to compare the simulation results. Figure 15 shows the results of the roll axis at 60knot forward flight. The point model (green) cannot predict the measured response though the oscillation is qualitatively predicted. The additive uncertainty together with the point model (blue) predicts the oscillation well.

8. APPLICATION TO FEEDBACK CONTROL DESIGN

The three parts (i.e. additive uncertainty, input uncertainty, and stitched model) are combined such that the overall model allows for performant feedback design. The model has the following state equation

$$\begin{aligned}
 \Delta \dot{\mathbf{x}} &= (\mathbf{A}(\xi_f) + \mathbf{A}_{a,\xi_{PID}}(\xi_f))(\mathbf{x} - \mathbf{x}_{t,f}) + \\
 &\quad (\mathbf{B}(\xi_f) + \mathbf{B}_{a,\xi_{PID}}(\xi_f))(\mathbf{u} - \mathbf{u}_t(\xi)) + \\
 &\quad \mathbf{f}(\mathbf{x}, \mathbf{u}) - \mathbf{f}(\mathbf{x}_t(\xi), \mathbf{u}_t(\xi))
 \end{aligned}
 \tag{18}$$

where the control inputs are obtained through

$$\mathbf{u} = \Delta_m \mathbf{u}_f + \mathbf{u}_f
 \tag{19}$$

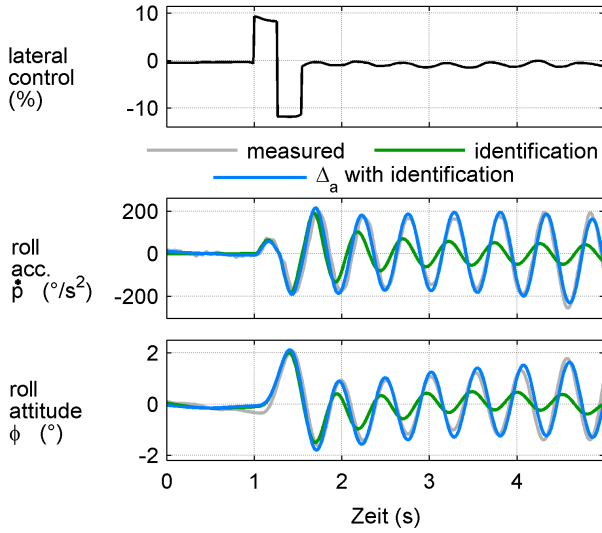


Figure 15: Roll rate due to lateral control at 60 knot forward flight of the ACT/FHS, measurements (grey) from flight test, point model with input uncertainty (green), and point model with additive and input uncertainty (blue)

\mathbf{u}_f denotes the processed controls that have been filtered to avoid structural oscillations of the fuselage and tailboom and that then have passed the core system computer as well as the actuators. A simple approximation of this signal processing is provided by

$$(20) \quad \mathbf{u}_f = -1/T_1 \dot{\mathbf{u}}_f + e^{-t/T_t} \mathbf{u}_c$$

The controls generated by feedback are called \mathbf{u}_c . The three models equations (18-20) are used for the feedback control design.

Example. Assume that system identification results in the model equations (11, 12) of the pitch attitude due to longitudinal control. Assume further that the control design results in a PID-controller with (SI-units are used)

$$(21) \quad \delta_{x,c} = 40 \dot{e} + 110 e + 50 \int e dt$$

with: $e = \theta_c - \theta$

The control signal $\delta_{x,c}$ is processed by equation (20) where the time constant is $T_1 = 25$ ms and the delay is $T_t = 25$ ms. With this, the closed-loop system as depicted in figure 16 is set up. The simulated closed-loop response with the feedback controller of equation (21) is shown in figure 17. The grey curve shows the commanded pitch attitude that is desired by the pilot. The blue curve shows the response expected by the design. The same closed-loop behavior is expected in real flight but, however, reveals a slightly oscillatory response (red curve). After application of the inverse simulation, the pitch axis requires the following input uncertainty (taken from the ACT/FHS correspondent input uncertainty):

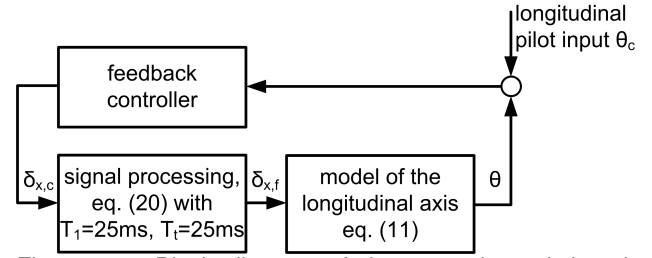


Figure 16: Block diagram of the exemplary pitch axis closed-loop

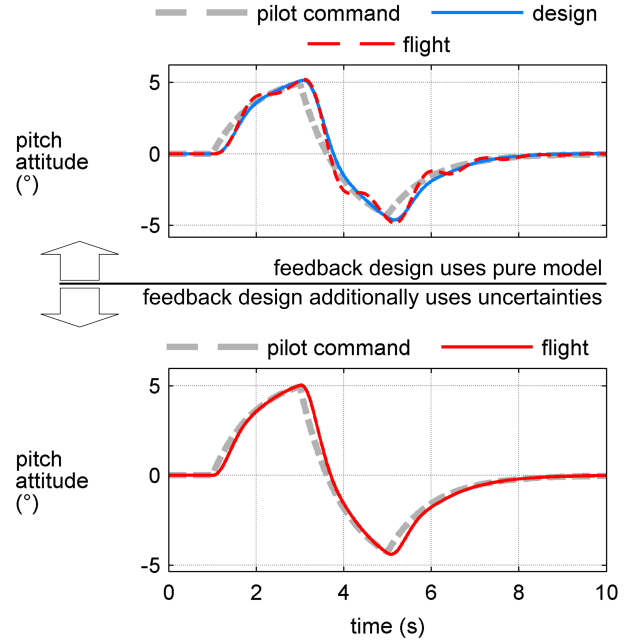


Figure 17: Closed-loop response of the pitch attitude for the pitch axis example

$$(22) \quad \Delta_m = \frac{-2.6 \cdot 10^5 s(s-10)}{(s+3)(s+0.3)(s^2+10s+925)(s^2+7s+1612)}$$

The controller design is now assisted through the modeling of the oscillation at approx. 35 rad/s. The controller design uses an additional feedback of the pitch acceleration to avoid the oscillating response of the pitch attitude. Assume that the controller design results in the following feedback controller:

$$(23) \quad \delta_{x,c} = 6 \ddot{e} + 60 \dot{e} + 110 e + 50 \int e dt$$

with: $e = \theta_c - \theta$

The respective closed-loop response (red continuous line) on bottom of figure 17 is similar to the preliminary expectation from the first design (blue curve in top of the same figure).

Application to ACT/FHS data. The whole procedure is applied to the ACT/FHS with its models derived by system

identification [8, 18]. The high-bandwidth control of the roll axis for instance is documented in references [13, 34]. By means of the additive uncertainty as shown in figure 15, the feedback design is tailored such that air resonance is suppressed and high-bandwidth control is possible. Figure 18 shows the comparison between high gain roll rate feedback (green) and the same feedback with additional air resonance suppression (red).

The framework is also applied to the pitch axis and helps to improve the response to pitch attitude. Similar to the example in equation (23), an additional feedback of the pitch acceleration is used. Compared to the example, the ACT/FHS has a much more complex on-axis pitch transfer function (due to coupling) and features feed-forward control [35]. Figure 19 shows the response obtained with the preliminary control architecture. The attitude is not well tracked although the feedback design by means of the original model leads to the expectation of an overall good tracking performance. Then, the whole framework with the full envelope model, input, and additive uncertainty was applied. Based on the adapted model of the plant, the feedback controller for the pitch axis was redesigned similar to the example given by equation (23). In flight tests, the redesigned feedback controller shows a significant improvement (figure 19).

The full envelope simulation equation (7) also helps in assessing the performance of the maneuvering flight. The perturbation about the trim controls for instance emphasizes that a deceleration maneuver depends on the stationary trim curve. The feedback cannot predict this effect so that a corresponding compensation is used. For the longitudinal PID-controller, the trim curve is compensated through:

$$(24) \quad \delta_{x,c} = K_{dd} \ddot{e} + K_d \dot{e} + K_p e + K_i \int e dt + \delta_{x,t}(V_a) - \delta_{x,t}(t=0)$$

with: $e = \theta_c - \theta$

The additional term $\delta_{x,t}(V_a) - \delta_{x,t}(t=0)$ avoids the steady-state tracking error which is shown in figure 20.

9. CONCLUSION AND OUTLOOK

The predicting capability of linear models is crucial for successful high-bandwidth feedback control. The approach presented in this paper relies on the combination of physics-based system identification and generic modeling and shows the application to feedback control design for simple examples as well as real flight tests with the ACT/FHS. The physics-based approach allows for full envelope modeling with linear models that are interpolated smoothly and respect nonlinear terms such as kinematics and trim curves. Advantageously, the maneuvering flight with deceleration and acceleration can be simulated and the feedback controller can be designed with respect to maneuvering flight.

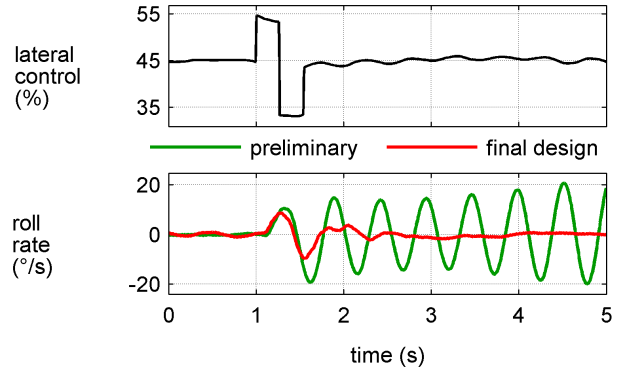


Figure 18: Application of the additive uncertainty to suppress air resonance of the ACT/FHS

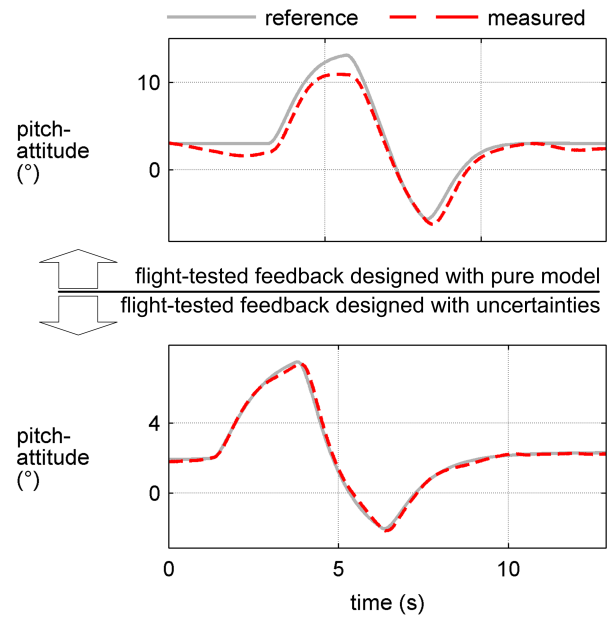


Figure 19: Design of the pitch attitude controller with and without input uncertainty

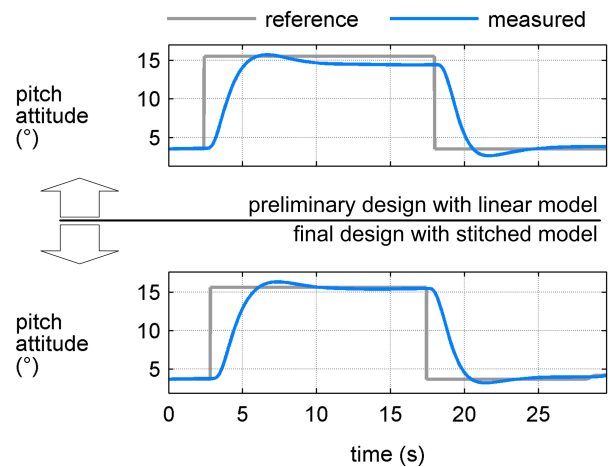


Figure 20: Pitch attitude control with classical PID (top) and with trim curve feedback (bottom)

Although, nonlinear remnants may be covered by the full envelope model, certain modeling uncertainties may still remain. Those uncertainties can be covered by adding the input and additive uncertainty which are derived by means of inverse simulation and partial closed-loop, respectively. Finally, the model of the plant consists of a full envelope helicopter simulation that is based on system identification results and enhanced by generic uncertainty models. The paper shows the advantage of this framework by recently flight-tested feedback control results and future work will apply this approach to next upcoming feedback design tasks. The results on the uncertainties shown in this paper will be transferred to the physics-based system identification which may then be improved in predicting the helicopter response. Additionally, generic system identification [36] will be performed and the results will be used to further improve the modeling.

ACKNOWLEDGEMENT

This work is made possible through the assistance by Dr.-Ing. W. v. Grünhagen (DLR, Institute of Flight Systems). I would like to thank him for his time, sharp words, encouragement and open ear throughout the last few years.

COPYRIGHT STATEMENT

The author confirms that his organization hold copyright on all of the original material included in this paper. The author also confirms that he has obtained permission, from the copyright holder of any third party material included in this paper, to publish it as part of his paper. The author confirms that he give permission, or has obtained permission from the copyright holder of this paper, for the publication and distribution of this paper as part of the ERF2015 proceedings or as individual offprints from the proceedings and for inclusion in a freely accessible web-based repository.

REFERENCES

- [1] J. Kaletka, H. Kurscheid, and U. Butter, "FHS, the New Research Helicopter: Ready for Service," *Aerospace Science and Technology*, vol. 9, no. 5, pp. 456–467, 2005.
- [2] R. Lantzs, S. Greiser, J. Wolfram, J. Wartmann, M. Müllhäuser, T. Lüken, H. U. Döhler, and N. Peinecke, "ALLFlight: A Full Scale Pilot Assistance Test Environment," in *American Helicopter Society 68th Annual Forum, Ft. Worth, TX*, May 1-3, 2012.
- [3] S. Greiser, R. Lantzs, J. Wolfram, J. Wartmann, M. Müllhäuser, T. Lüken, H. U. Döhler, and N. Peinecke, "Results of the Pilot Assistance System "Assisted Low-Level Flight and Landing on Unprepared Landing Sites" Obtained with the ACT/FHS Research Rotorcraft," *Aerospace Science and Technology*, vol. 45, pp. 215–227, 2015.
- [4] T. Schönenberg, "Design of a Conceptual Rotorcraft Model Preparing Investigations of Sidestick Handling Qualities," in *American Helicopter Society 67th Annual Forum, Virginia Beach, Virginia*, May 3-5, 2011.
- [5] F. M. Nieuwenhuizen, M. Jump, P. Perfect, M. D. White, G. D. Padfield, D. Floreano, F. Schill, J. C. Zuferey, P. Fua, S. Bouabdallah, R. Siegwart, S. Meyer, J. Schippl, M. Decker, B. Gursky, M. Höfinger, and H. H. Büthoff, "myCopter – Enabling Technologies for Personal Aerial Transportation Systems," in *3rd International HELI World Conference*, pp. 1–8, 2011.
- [6] B. Benoit, A. M. Dequin, P. M. Basset, B. Gimonet, W. von Grünhagen, and K. Kampa, "HOST, a General Helicopter Simulation Tool for Germany and France," in *American Helicopter Society 56th Annual Forum, Virginia Beach, Virginia*, May 2-4, 2000.
- [7] M. Hamers and W. von Grünhagen, "Nonlinear Helicopter Model Validation Applied to Realtime Simulations," *Forum of the American Helicopter Society*, 1997.
- [8] S. Seher-Weiss and W. von Grünhagen, "EC135 System Identification for Model Following Control and Turbulence Modeling," in *Proceedings of the 1st CEAS European Air and Space Conference, Berlin*, pp. 2439–2447, 2007.
- [9] M. B. Tischler and R. K. Remple, *Aircraft and Rotorcraft System Identification: Engineering Methods with Flight Test Examples*. Reston, VA: American Institute of Aeronautics and Astronautics, 2 ed., 2012.
- [10] C. M. Ivler and M. B. Tischler, "Case Studies of System Identification Modeling for Flight Control Design," *Journal of The American Helicopter Society*, vol. 58, no. 1, pp. 1–16, 2013.
- [11] S. Seher-Weiss and W. von Grünhagen, "Comparing Explicit and Implicit Modeling of Rotor Flapping Dynamics for the EC135," in *Deutscher Luft- und Raumfahrtkongress, Berlin*, September 10-12, 2012.
- [12] C. M. Ivler and M. B. Tischler, "System Identification Modeling for Flight Control Design," in *RAeS Rotorcraft Handling-Qualities Conference, University of Liverpool, UK*, November 4-6, 2008.
- [13] S. Greiser, "Disturbance Observer-Based Control to Suppress Air Resonance for the EC135 ACT/FHS Research Helicopter," in *AIAA SciTech, Modeling and*

Simulation Technologies Conference, Kissimmee, FL, USA, Januar 5-9, 2015.

- [14] J. C. Antonioli, A. Taghizad, T. Rakotomamonjy, and M. Ouladsine, "Toward the Development of a Methodology for Designing Helicopter Flight Control Laws by Integrating Handling Qualities Requirements," in *40th European Rotorcraft Forum, Southampton, UK*, September 2-5, 2014.
- [15] B. Mueller, *Ein Beitrag zur Bestimmung der Fluggeschwindigkeit von Hubschraubern mit Zustandsbeobachtern*. Braunschweig: DFVLR, Institut für Flugführung, 1987.
- [16] H. Leyendecker, *Ein Beitrag zur dynamischen Vorsteuerung von Mehrgrößensystemen und zur optimalen Gestaltung von Führungsgrößen*. Braunschweig: DFVLR, Institut für Flugführung, 1992.
- [17] L. Zivan and M. B. Tischler, "Development of a Full Flight Envelope Helicopter Simulation Using System Identification," *Journal of The American Helicopter Society*, vol. 55, 2010.
- [18] S. Greiser and S. Seher-Weiss, "A Contribution to the Development of a Full Flight Envelope Quasi-Nonlinear Helicopter Simulation," *CEAS Aeronautical Journal*, 2013.
- [19] E. L. Tobias, M. B. Tischler, T. Berger, and S. G. Hagerott, "Full Flight-Envelope Simulation and Piloted Fidelity Assessment of a Business Jet Using a Model Stitching Architecture," in *AIAA SciTech, Modeling and Simulation Technologies Conference, Kissimmee, FL, USA*, Januar 5-9, 2015.
- [20] J. Hodgkinson, *Aircraft Handling Qualities*. Reston, VA: AIAA Educational Series, 1998.
- [21] R. E. Smith, J. Hodgkinson, and R. C. Snyder, *Equivalent System Verification and Evaluation of Augmentation Effects on Fighter Approach and Landing Flying Qualities: AFWAL-TR-81-3116*, vol. 2. Wright-Patterson Air Force Base, OH: U.S. Air Force, Wright Aeronautical Lab., 1981.
- [22] D. J. Murray-Smith and B. O. Wong, "Inverse Simulation Techniques Applied to the External Validation of Nonlinear Dynamic Models," in *Third Conference of the United Kingdom Simulation Society, Edinburgh, UK*, pp. 100–104, April, 1997.
- [23] D. G. Thomson and R. Bradley, "The Principles and Practical Application of Helicopter Inverse Simulation," *Simulation Practice and Theory*, vol. 6, pp. 47–70, 1998.
- [24] W. von Grünhagen, "Inverse Simulation: a Tool for the Validation of Simulation Programs - First Results," *Zeitschrift für Flugwissenschaften und Weltraumforschung*, vol. 17, pp. 211–219, 1993.
- [25] S. Greiser and W. von Grünhagen, "Analysis of Model Uncertainties Using Inverse Simulation," in *American Helicopter Society 69th Annual Forum, Phoenix, AZ*, May 21-23, 2013.
- [26] M. Hamers, R. Lantzsich, and J. Wolfram, "First Control Evaluation of Research Helicopter FHS," in *33rd European Rotorcraft Forum, Kazan, Russia*, September 11-13, 2007.
- [27] R. Lantzsich, J. Wolfram, and M. Hamers, "Increasing Handling Qualities and Flight Control Performance using an Air Resonance Controller," in *American Helicopter Society 64th Annual Forum, Montréal, Canada*, April 29 - May 1, 2008.
- [28] G. J. Gray and W. von Grünhagen, "An Investigation of Open-Loop and Inverse Simulation as Nonlinear Model Validation Tools for Helicopter Flight Mechanics," *Mathematical and Computer Modeling of Dynamical Systems*, vol. 4, no. 1, pp. 32–57, 1998.
- [29] P. Krämer, *Hybridmodellierung und Systemidentifizierung der nichtlinearen Hubschrauber-Flugdynamik*. Braunschweig: DLR, Institut für Flugsystemtechnik, 2006.
- [30] S. Skogestad and I. Postlethwaite, *Multivariable Feedback Control: Analysis and Design*. Chichester: John Wiley & Sons, 2005.
- [31] E. G. Rynaski, "Adaptive Multivariable Model Following," in *Joint Automatic Control Conference, San Francisco, CA*, August 13-15, 1980.
- [32] S. Seher-Weiss, *User's Guide FITLAB: Parameter Estimation Using MATLAB, Version 2.1, basiert auf IB 111-2007/27*. 2009.
- [33] M. Marchand and K. H. Fu, "Frequency Domain Parameter Estimation of Aeronautical Systems with and without Time Delay," in *Proceedings of the 7th IFAC Symposium on Identification and System Parameter Estimation, York, UK*, pp. 669–674, July 3-7, 1985.
- [34] S. Greiser and R. Lantzsich, "Equivalent Modelling and Suppression of Air Resonance for the ACT/FHS in Flight," in *39th European Rotorcraft Forum, Moscow, Russia*, September 3-6, 2013.
- [35] J. Wartmann, "Model Validation and Analysis Using Feedforward Control Flight Test Data," in *Deutscher Luft- und Raumfahrtkongress, Berlin*, September 10-12, 2012.
- [36] J. Wartmann and S. Seher-Weiss, "Application of the Predictor-Based Subspace Identification Method to Rotorcraft System Identification," in *39th European Rotorcraft Forum, Moscow, Russia*, September 3-6, 2013.